PPARG directs trophoblast cell fate and establishment of the uterine-placental interface

Esteban M. Dominguez[1,*], Ayelen Moreno-Irusta[1], Khursheed Iqbal[1ψ], Keting Chen[2], Alex Finlinson[3], Marc Parrish[3], Hiroaki Okae[4], Takahiro Arima[5], Geetu Tuteja[2], and Michael J. Soares[1,3,*]

[1]Institute for Reproductive and Developmental Sciences, Department of Pathology & Laboratory Medicine, University of Kansas Medical Center, Kansas City, KS 66160, USA,[2]Department of Genetics, Development, and Cell Biology, Iowa State University, Ames, IA 50011,USA, [3]Department of Obstetrics and Gynecology, University of Kansas Medical Center, Kansas City, KS 66160,USA,[4]Department of Trophoblast Research, Institute of Molecular Embryology and Genetics, Kumamoto University, Kumamoto 860-0811, Japan,[5]Department of Informative Genetics, Environment and Genome Research Center, Tohoku University Graduate School of Medicine, and Department of Molecular Oncology, Institute of Development, Aging and Cancer, Tohoku University, Sendai 980-8575, Japan

[ψ]Present address: Department of Animal & Food Science, Oklahoma State University, Stillwater, OK 74078, USA.

***Corresponding authors:** Esteban M. Dominguez, edominguez@kumc.edu or Michael J. Soares, msoares@kumc.edu

3901 Rainbow Blvd. Kansas City, KS 66160, USA, Mail Stop 3050.

Phone: 913 588 5960 or 913 588 5961.

Abstract

The expansion and differentiation of trophoblast stem (**TS**) cells are critical for defining fundamental properties of the placenta. Specialized trophoblast cells exit the placenta and enter and transform the uterus, including restructuring uterine spiral arteries. In the human these cells are named extravillous trophoblast (**EVT**) cells, whereas in the rat they are termed invasive trophoblast cells. Mechanisms governing invasive trophoblast cell differentiation remain poorly understood. We investigated peroxisome proliferator-activated receptor gamma (**PPARG**) as a potential regulator of EVT/invasive trophoblast cell development. In first trimester human placentas, PPARG was expressed in the EVT cell column and increased in amount as human TS cells differentiated into EVT cells. PPARG disruption impaired EVT cell differentiation. Rat invasive trophoblast cells similarly expressed PPARG. Conditional inactivation of PPARG within rat invasive trophoblast cells was used to assess the in vivo role of PPARG on the uterine-placental interface. PPARG was established as an essential cell-autonomous regulator of the invasive trophoblast cells. In conclusion, PPARG is a conserved regulator of placentation and is essential for directing trophoblast cell-guided uterine transformation.

Keywords: hemochorial placenta/PPARG/trophoblast cell invasion/uterine remodeling/ pregnancy.

Introduction

The uterine-placental interface is a dynamic site where uterine and placental structures cooperate to establish a protective environment that redirects maternal resources to support embryonic and fetal development (Georgiades *et al*, 2002; Maltepe & Fisher, 2015). Both humans and rats possess a hemochorial placenta, characterized by deep trophoblast cell invasion into the uterine parenchyma and remodeling of the uterine vasculature to ensure optimal maternal blood supply to the placenta (Pijnenborg *et al*, 1981; Soares *et al*, 2012). This vascular transformation is critical for successful pregnancy (Pijnenborg *et al*, 2006; Aye *et al*, 2025). Impairments in this process can lead to complications such as pregnancy loss, preeclampsia, intrauterine growth restriction, and preterm birth (Aye *et al*, 2025; Brosens *et al*, 2011; Fisher, 2015; Brosens *et al*, 2019; Harris *et al*, 2019). These complications significantly contribute to maternal and fetal morbidity and mortality (Fisher, 2015; Brosens *et al*, 2019; Kaufmann *et al*, 2003). Furthermore, suboptimal intrauterine conditions can trigger fetal adaptations that increase susceptibility to disease later in life (Calkins & Devaskar, 2011; Gluckman *et al*, 2008).

Throughout gestation, maternal blood flows into the placenta, delivering essential nutrients and oxygen to support fetal development. As pregnancy progresses, maternal uterine spiral arteries are remodeled into distended, low-resistance vessels capable of meeting the increasing demands of the growing fetus (Kaufmann *et al*, 2003; Harris, 2010). At the core of spiral artery remodeling are invasive trophoblast cells, referred to as extravillous trophoblast (**EVT**) cells in the human (Velicky *et al*, 2015). These cells take two routes into the uterus. They migrate inside the uterine vasculature and within the uterine stroma situated between uterine blood vessels and are referred to as endovascular invasive trophoblast/EVT cells and interstitial invasive trophoblast/EVT cells, respectively. Endovascular invasive trophoblast/EVT cells replace endothelial cells and adopt a pseudo-endothelial phenotype (Hemberger *et al*, 2003; Rai & Cross,

65 2014). Given the critical role of invasive trophoblast/EVT cells in uterine spiral artery remodeling,
66 it is crucial to identify mechanisms that regulate invasive trophoblast/EVT cell development.
67
68 Peroxisome proliferator-activated receptor gamma (**PPARG**) is a member of the nuclear
69 hormone receptor superfamily of ligand-activated transcription factors (Sauer, 2015). PPARG is
70 essential for placental development in the mouse (Barak *et al*, 1999; Kubota *et al*, 1999).
71 Deficiency of PPARG results in embryonic lethality at mid-gestation (Barak *et al*, 1999; Kubota *et*
72 *al*, 1999). In addition, PPARG is expressed in the human placenta and is involved in human
73 trophoblast cell development and regulating key placental functions (Schaiff *et al*, 2006; Tarrade,
74 2001; Tarrade *et al*, 2001; Pavan *et al*, 2003; Fournier *et al*, 2007; Schaiff *et al*, 2000; Shalom-
75 Barak *et al*, 2004). Among its diverse actions on placentation is its potential involvement in
76 regulating the invasive trophoblast cell lineage. Within rat and human placentation sites, PPARG
77 is prominently expressed in invasive trophoblast/EVT cell lineages (Liu *et al*, 2018; Vento-Tormo
78 *et al*, 2018; Scott *et al*, 2022). PPARG dysregulation is also evident in diseases associated with
79 failures in trophoblast cell-guided uterine spiral artery remodeling such as preeclampsia and
80 intrauterine growth restriction (Rodie *et al*, 2005; Waite *et al*, 2005; Holdsworth-Carson *et al*,
81 2010).
82
83 In this study, we investigated the involvement of PPARG on EVT cell lineage development in
84 vitro using human trophoblast stem (**TS**) cells. Human TS cells are a robust in vitro model system
85 and have provided new insights into the regulation of trophoblast cell differentiation (Okae *et al*,
86 2018; Varberg *et al*, 2023). The contributions of PPARG to invasive trophoblast cell development
87 were also examined in vivo using a conditionally disrupted *Pparg* rat model. Our findings
88 demonstrate that PPARG is a critical and conserved regulator of invasive trophoblast cell
89 development and invasive trophoblast cell-guided transformation of the uterine vasculature.

Results

PPARG is expressed in EVT cells

Distributions of PPARG transcript and protein in first trimester human placenta tissue were determined by in situ hybridization and immunohistochemistry, respectively. PPARG transcript (Fig. 1A) and protein (Fig. 1B) were ubiquitously expressed throughout trophoblast cells within villous and extravillous compartments of the human placenta, including EVT cells. The transcript for notum, palmitoleoyl protein carboxylesterase (**NOTUM**), an EVT cell-associated transcript (Shukla *et al*, 2024), co-localized with PPARG transcripts in the distal region of the EVT cell column (Fig. 1A). PPARG protein was located within nuclei of EVT cells (Fig. 1B). These observations are consistent with previous reports (Tarrade *et al*, 2001; Waite *et al*, 2000). PPARG expression was also examined in CT27 (X,X) human TS cells, in the stem state and after EVT cell differentiation (Okae *et al*, 2018). Expression of *TEAD4* and *TP63* defined the stem state of these cells, whereas *HLA-G* and *MMP2* expression characterized EVT cell differentiation (Fig. EV1A). PPARG transcript and protein expression increased from the stem state to EVT cell differentiation state (Fig. 1C). Thus, PPARG is expressed in EVT cells of the developing human placenta and in human EVT cells following their differentiation from TS cells.

PPARG effects on EVT cell differentiation

The expression of PPARG within EVT cells prompted an investigation into a possible role for PPARG in EVT cell development. A lentiviral-mediated short hairpin RNA (**shRNA**) loss-of-function strategy was used to inhibit PPARG in CT27 (X,X) TS cells. PPARG transcript and protein were significantly decreased in EVT cells stably expressing either of two different PPARG shRNAs when compared to expression of a control shRNA (Fig. 2A). The specificity of PPARG-targeting shRNAs was assessed by monitoring the expression of other members of the PPAR family. Expression of *PPARA* and *PPARD* transcripts were not affected following treatment with PPARG shRNAs (Fig. EV1B). Treatment with PPARG shRNAs slowed TS cell proliferation without changes in stem state associated markers TEAD4 and TP63 (Fig. EV1C-E). Disruption of PPARG affected the morphology of the EVT cell differentiation state, including a decrease in cell elongation and the

118 presence of stem state-like cell clusters (Fig. 2B). Cells expressing PPARG shRNAs showed
119 significantly less migration than EVT cells expressing a control shRNA (Fig. 2C). Similar findings
120 were observed in CT29 (X,Y) TS cells following their manipulation with PPARG shRNAs (Fig.
121 EV2A-C). Additionally, exposure to a small molecule PPARG antagonist (GW9662) similarly
122 negatively affected stem state proliferation, EVT cell differentiation, and cell migration (Fig. EV3A-
123 J**)**. Collectively, the findings indicate that PPARG possesses a fundamental role in regulating EVT
124 cell development and function.
125
126 *PPARG effects on trophoblast organoids*
127 We next examined the involvement of PPARG in establishment and behavior of TS cell-derived
128 trophoblast organoids. We initially validated the TS cell-derived trophoblast organoid culture
129 system (Fig. EV 4A–D) and then examined control or PPARG deficient trophoblast organoids. The
130 ability to form trophoblast organoids was not affected by PPARG disruption (Fig. 3A); however,
131 PPARG inhibition did affect EVT cell differentiation from trophoblast organoids (Fig. 3B). This
132 finding was supported by inspection of the morphology of the trophoblast organoids and their
133 expression of TS cell stem state transcripts (*TEAD4, TFAP2C, TP63, CDH1*) and EVT cell-
134 associated transcripts (*MMP15, HLA-G, FSTL3, ASCL2, DLX6, PLAC8*) (Fig. 3C).
135
136 *Identification of PPARG gene targets in EVT cells*
137 PPARG is a transcription factor, which prompted an examination of transcripts affected by
138 PPARG disruption. RNA sequencing (**RNA-seq**) was performed, and transcriptomic profiles
139 analyzed following eight days of EVT cell differentiation in control shRNA and PPARG1 shRNA
140 treated cells (Appendix Dataset 1**)**. A total of 5,845 differentially expressed genes were identified
141 in control versus PPARG1 shRNA treated cells ($p<0.05$, and fold change of 1.5), including 2,510
142 upregulated and 3,335 downregulated genes. The differential gene expression profile is presented
143 as a volcano plot (Fig. 4A). Selected upregulated and downregulated genes connected to
144 trophoblast cell biology are shown in a heat map (Fig. 4B). We identified upregulation of several
145 genes associated with the TS cell stem state (e.g. *TEAD4, TFAP2C, TP63, CDH1*) and

146 downregulation of several EVT cell-associated genes (e.g. *ITGA1, ITGAV, FLT1, EPAS1, DLX6,*
147 *PLAC8, TFPI, FSTL3*). These findings were independently validated by reverse transcriptase-
148 quantitative polymerase chain reaction (**RT-qPCR,** Fig. 4C, Appendix Fig.1**).** Gene ontology (**GO**)
149 (Fig. 4D and Appendix Dataset 2,3) and gene set enrichment analysis (**GSEA**) (Fig. 4E and
150 Appendix Dataset 4) implicated PPARG in the upregulation of cell cycle associated genes and the
151 downregulation of cell projection assembly associated genes. The latter cellular process directly
152 connects PPARG with cell elongation and motility that are acquired as TS cells transit from the
153 stem state to EVT cells.
154
155 Since, PPARG is a transcription factor, we next analyzed genome-wide PPARG-DNA
156 interactions using chromatin immunoprecipitation sequencing (**ChIP-seq**). We identified 7,319
157 genes with at least one PPARG bound region (peak) in differentiated EVT cells (Appendix Dataset
158 5). The two most prevalent motifs identified within the peaks were known PPARG DNA binding
159 motifs (peroxisome proliferator response element, **PPRE**) and primarily consisted of a direct repeat
160 1 (**DR1**) sequence (Fig. 5A). Most PPARG-DNA peaks (~7000) were located within introns or
161 intergenic regions of protein-coding genes (Fig. 5B,C), suggesting the involvement of PPARG in
162 the regulation of enhancer activity. Integration of RNA-seq (5,845 differentially expressed genes)
163 and ChIP-seq (7,319 genes with PPARG peak) datasets resulted in the identification of 2,512
164 potential direct PPARG gene targets (Fig. 5D, Appendix Dataset 6). GO analyses of PPARG gene
165 targets identified by PPARG ChIP-seq (Fig. 5E, Appendix Dataset 7) and an integrated dataset of
166 PPARG responsive genes identified by RNA-seq of EVT cells (see Fig. 4) and PPARG gene targets
167 identified by PPARG ChIP-seq (Fig. 5F, Appendix Dataset 8) prominently identified genes
168 associated with positive regulation of cell projection organization and tissue migration. These
169 represent cellular processes associated with EVT cell differentiation. In addition, GO analysis
170 identified PPARG target genes connected to response to hypoxia, lipid transport, and WNT
171 signaling, which are also likely important in the transition from the stem state to mature
172 differentiated EVT cells (Fig. 5E). Evidence supporting *PLAC8*, *TFPI*, *DLX6*, *FSTL3* and *TP63*,
173 which are known regulators of trophoblast cell differentiation (Chang *et al*, 2018; Xie *et al*, 2018;

174 Muto *et al*, 2021; Wang *et al*, 2022; Kim *et al*, 2024), as potential direct targets of PPARG is shown
175 (Fig. 5G). Collectively, the results support PPARG regulating genes that control development of
176 the EVT cell lineage.
177
178 *PPARG expression within the rat uterine-placental interface*
179 The rat exhibits deep intrauterine trophoblast cell invasion (Ain *et al*, 2003), a feature of
180 placentation also observed in the human, and has proven to be a useful in vivo model for
181 investigating the physiological relevance of genes implicated in the regulation of the invasive
182 trophoblast cell lineage (Chakraborty *et al*, 2016; Varberg *et al*, 2021; Muto *et al*, 2021; Kuna *et al,*
183 2023; Dominguez *et al,* 2024). We next sought to determine whether PPARG was expressed in
184 trophoblast cells of the rat placenta, especially within invasive trophoblast cells of the rat uterine-
185 placental interface. The rat placentation site is organized into three main compartments: i) labyrinth
186 zone, ii) junctional zone, and iii) uterine-placental interface (Soares *et al*, 2012; Shukla & Soares,
187 2022). The labyrinth zone is comprised of trophoblast cells and fetal vasculature and represents
188 the site of maternal-fetal exchange, whereas the junctional zone contains several trophoblast cell
189 types, including invasive trophoblast cell progenitors, which direct pregnancy-dependent
190 adaptations of maternal tissues. The uterine-placental interface is the uterine compartment
191 adjacent to the placenta where invasive trophoblast cells, uterine vasculature, and maternal
192 immune cells are situated. *In situ* hybridization was used to determine the distribution of *Pparg*
193 transcripts. At gestation day (**gd**) 11.5, *Pparg* transcripts were localized to trophoblast cells of the
194 developing placenta as well as to invasive trophoblast cells situated within uterine spiral arteries
195 (Fig. 6A). The presence of *Pparg* transcripts in trophoblast cells was confirmed by co-localization
196 with keratin 8 (*Krt8*), an epithelial cell associated transcript expressed by trophoblast cells (Fig. 6A).
197 By gd 18.5, *Pparg* was expressed within trophoblast cells of the labyrinth zone, junctional zone,
198 and within invasive trophoblast cells of the uterine–placental interface (Fig. 6B). Expression of
199 *Pparg* in invasive trophoblast cells was supported by its co-localization with prolactin family 7,
200 subfamily b, member 1 (***Prl7b1*,** Fig. 6B,C), an invasive trophoblast cell-associated transcript (Scott
201 *et al*, 2022; Wiemers *et al*, 2003). These findings are consistent with a previously published report

202 describing single cell RNA-seq analysis of the rat uterine–placental interface, which demonstrated
203 that *Pparg* expression was enriched in the invasive trophoblast cell lineage (Appendix Fig. 2, Scott
204 *et al*, 2022). *Pparg* transcript levels increased within the uterine–placental interface as pregnancy
205 progressed (Fig. 6D). Furthermore, PPARG protein was localized to invasive trophoblast cells and
206 throughout the junctional and labyrinth zones, as shown by immunohistochemistry (Fig. 6E). Thus,
207 PPARG expression is a conserved feature of EVT cells of the human placenta (Fig. 1) and invasive
208 trophoblast cells of the rat placentation site (Fig. 6).
209
210 *Establishment and validation of the invasive trophoblast cell-specific Pparg mutant rat*
211 Next, we examined an in vivo role for PPARG in development of rat invasive trophoblast cells.
212 Since, PPARG is expressed in trophoblast cell lineages throughout the rat placentation site (Fig.
213 6B) and global inactivation of the mouse *Pparg* gene was associated with midgestation lethality
214 (Barak *et al*, 1999; Kubota *et al*, 1999), we utilized a conditional Cre/Lox approach to selectively
215 disrupt *Pparg* in the invasive trophoblast cell lineage. For these experiments we used a rat model
216 possessing Cre recombinase inserted into the *Prl7b1* locus. As noted above, *Prl7b1* is robustly and
217 specifically expressed within invasive trophoblast cells of the rat placentation site (Wiemers *et al*,
218 2003; Scott *et al*, 2022; Iqbal *et al*, 2024). The *Prl7b1-Cre* specifically acts within the invasive
219 trophoblast cell lineage without anomalous activities in non-invasive trophoblast cells or other
220 extraembryonic and embryonic tissues (Dominguez *et al, 2024*; Iqbal *et al*, 2024). Male *Prl7b1-Cre*
221 rats and female rats possessing *loxp* sites flanking Exons 2 and 3 of the *Pparg* gene (Fig. 7A) were
222 used in the analysis. Specifically, *Prl7b1-Cre*/heterozygous floxed *Pparg* (***Prl7b1***^{Cre}***/Pparg***$^{f/+}$) males
223 were mated with homozygous floxed *Pparg* female rats (***Pparg***$^{f/f}$) to generate *Pparg*$^{f/f}$ and *Pparg*
224 deleted (***Pparg***$^{d/d}$) placentation sites. Immunohistochemical analysis for PPARG demonstrated the

225 presence of PPARG protein at the gd 18.5 uterine–placental interface of *Pparg*$^{f/f}$ but not within this
226 compartment of *Pparg*$^{d/d}$ placentation sites (Fig. 7B).
227
228 *PPARG involvement in rat invasive trophoblast cell lineage development and cellular dynamics*
229 *within the uterine-placental interface*
230 The structure and integrity of *Pparg*$^{f/f}$ and *Pparg*$^{d/d}$ placentation sites were different. An
231 expanded decidual compartment was evident within *Pparg*$^{d/d}$ placentation sites (Fig. 7C). *Pparg*$^{d/d}$
232 placentas were larger (Fig. 7C), possessed an enlarged junctional zone (Fig. EV5) containing
233 prominent cyst-like structures (Fig. 7C), and were less efficient than *Pparg*$^{f/f}$ placentas (Fig. 7D**)**.
234 Invasive trophoblast cells arise from the junctional zone (Soares *et al*, 2012; Shukla & Soares,
235 2022) and exhibited pronounced differences between *Pparg*$^{f/f}$ and *Pparg*$^{d/d}$ placentation sites (Fig.
236 8).
237
238 The uterine-placental interface of *Pparg*$^{f/f}$ placentation sites was infiltrated with invasive
239 trophoblast cells, which was not observed in *Pparg*$^{d/d}$ placentation sites, as detected by in situ
240 hybridization for *Prl7b1* or pan-cytokeratin immunostaining (Fig. 8A,B). Deficits in intrauterine
241 trophoblast cell invasion correlated with diminished expression of invasive trophoblast cell-
242 associated transcripts (*Prl5a1*, *Prl7b1*, *Krt8, Krt7, Cited2, Peg3, and Tfpi*) and pan-cytokeratin
243 immunoreactive surface area within the uterine-placental interfaces of *Pparg*$^{d/d}$ placentation sites
244 (Fig. 8C,D; Appendix Fig. 3). Previously published single cell RNA-sequencing and single nucleus
245 assay for transposase-accessible chromatin-sequencing datasets (Scott *et al*, 2022; Vu *et al*, 2023)
246 were used to reveal a network of genes potentially regulated by PPARG in rat invasive trophoblast
247 cells. These putative PPARG targets include candidate contributors to remodeling the extracellular
248 matrix, regulation of cell movement, cytoskeletal restructuring, and transcriptional regulators that

249 act on genes encoding other proteins affecting the invasive trophoblast cell phenotype (Appendix
250 Table 1 and Dataset 9).
251
252 Diminished intrauterine trophoblast cell invasion in *Pparg*$^{d/d}$ placentation sites was
253 accompanied by a retention of natural killer (**NK**) cells within the uterine-placental interface (Fig.
254 8E) and increased expression of NK cell-associated transcripts (Fig. 8F). NK cells are known
255 contributors to uterine spiral artery remodeling (Chakraborty *et al*, 2011; Rätsep *et al*, 2015; Renaud
256 *et al*, 2017; Erlebacher, 2013) but were less effective than invasive trophoblast cells in disabling
257 smooth muscle cells associated with uterine spiral arteries than invasive trophoblast cells (Fig.
258 8G,H).
259
260 Overall, these results highlight a key role for PPARG in directing development of the invasive
261 trophoblast cell lineage and the important role that invasive trophoblast cells possess in regulating
262 the cell composition and function of the uterine-placental interface.
263
264 **Discussion**
265 Hemochorial placentation serves the important function of delivering nutrients to ensure
266 coordinated on-time growth and development of the fetus within the female reproductive tract
267 (Soares *et al*, 2018). This type of placentation is found in many primates and rodents, including
268 the human and rat (Carter & Enders, 2004; Roberts *et al*, 2016). These two species exhibit
269 extensive invasive trophoblast cell-guided uterine transformation, including restructuring of spiral
270 arteries, which is fundamental to acquisition of maternal resources required for fetal development
271 (Pijnenborg *et al*, 1981). We examined a role for PPARG in development of invasive trophoblast
272 cells using human TS cells and a genetically manipulated rat model. In human placentation,
273 PPARG was expressed in EVT cell column cells and was shown to coordinate the upregulation of
274 genes required for cell elongation and the process of EVT cell movement. In the rat, PPARG was
275 expressed throughout the placenta, including invasive trophoblast cells, and was essential for
276 development of the invasive trophoblast cell lineage. Failures in PPARG-mediated gene

277 activation also affected human TS cell proliferation and led to abnormalities within compartments
278 of the rat placenta. The experimentation demonstrated that PPARG is a conserved regulator of
279 invasive trophoblast cell development and function.
280
281 Earlier research connected PPARG to placentation (Schaiff *et al*, 2006; Fournier *et al*, 2011;
282 Kadam *et al*, 2015). Insights regarding PPARG actions in placentation were unequivocally
283 demonstrated from analysis of global PPARG null mouse models (Barak *et al*, 1999; Kubota *et al*,
284 1999). PPARG disruption led to midgestation lethality due to an impairment of early events in
285 placental morphogenesis (Barak *et al*, 1999; Kubota *et al*, 1999). Considerable effort has also
286 been directed towards analyses of roles for PPARG in regulating trophoblast cells using an
287 assortment of in vitro models. PPARG deficient mouse TS cells exhibit impairments in
288 proliferation and syncytiotrophoblast development and enhanced trophoblast giant cell
289 differentiation (Parast *et al*, 2009), whereas human cytotrophoblast exposure to PPARG agonists
290 promoted syncytiotrophoblast formation and trophoblast cell-lipid accumulation, while inhibiting
291 trophoblast cell invasive properties (Tarrade, 2001; Tarrade *et al*, 2001; Schaiff *et al*, 2005). Our
292 in vitro and in vivo experimentation supported an essential role for PPARG in EVT/invasive
293 trophoblast cell lineage development. Similar observations of the involvement of PPARG in EVT
294 cell differentiation have recently been reported (Guo *et al*, 2025). Exposure to a PPARG
295 antagonist supported the involvement of PPARG actions in promoting EVT cell differentiation.
296 These PPARG actions on the EVT/invasive trophoblast cell lineage differ from observations with
297 PPARG activating ligands. PPARG can act independent of ligand and its actions can vary
298 depending upon the ligand investigated and may differ depending on the developmental state of
299 the target cells examined (Sauer, 2015). Thus, PPARG is a broad-spectrum regulator of placental
300 biology with critical actions on development of the EVT/invasive trophoblast cell lineage.
301
302 As indicated above, PPARG is expressed in multiple trophoblast cell lineages (Barak *et al*,
303 1999; Tarrade, 2001; Fournier *et al*, 2007; Waite *et al*, 2005; Asami-Miyagishi *et al*, 2004). Each
304 trophoblast cell lineage is responsible for controlling tasks critical for the development and

305 function of the placenta (Soares *et al*, 2018). Context is important. PPARG actions are not only
306 determined by its presence but also by the complement of posttranslational modifiers,
307 heterodimerization binding partners, and co-regulators expressed by a cell (Berger & Moller,
308 2002; Feige *et al*, 2006; Ahmadian *et al*, 2013).
309
310 In addition to PPARG, several other proteins have been shown to contribute to the regulation
311 of EVT cell differentiation. ASCL2, CITED2, DLX5, DLX6, EPAS1, GCM1, NOTUM, NRIP1,
312 SNAI1, TFAP2C, TFPI, WWTR1, and ZNF439, are required for optimal transition from the TS
313 cell stem state to EVT cells (Varberg *et al*, 2023; Shukla *et al*, 2024; Varberg *et al*, 2021; Muto *et*
314 *al*, 2021; Kuna *et al,* 2023; Kim *et al*, 2024; Jeyarajah *et al,* 2022; Meinhardt *et al,* 2025). A
315 *CRISPR* screen identified additional transcription factors contributing to the regulation of human
316 TS cells (Shimizu *et al*, 2023). The screen demonstrated the involvement of PPARG in the control
317 of TS cell proliferation, which was consistent with our observations, but not EVT cell
318 differentiation. The *CRISPR* screen utilized HLA-G expression as a method for monitoring EVT
319 cell differentiation. PPARG does not significantly affect HLA-G gene expression, which may
320 account for differences in the outcome of the *CRISPR* screen versus our findings. Based on
321 RNA-seq and ChIP-seq experiments we can place PPARG in a potential hierarchy of
322 transcription factors controlling EVT cell development (Appendix Fig. 4, Varberg *et al*, 2023,
323 2021; Kuna *et al,* 2023; Kim *et al*, 2024; Jeyarajah *et al,* 2022; Guo *et al*, 2025). Among the
324 regulators impacting EVT cell differentiation, ASCL2, TFPI, CITED2, TFAP2C and PPARG
325 possess conserved actions promoting development of the invasive trophoblast cell lineage in the
326 rat (Varberg *et al*, 2021; Muto *et al*, 2021; Kuna *et al*, 2023; Dominguez *et al*, 2024).
327
328 PPARG deficiency was associated with failed trophoblast cell invasion into the uterus leading
329 to a dramatic reorganization of the rat placentation site. The reorganization included the retention
330 of NK cells within the uterine-placental interface, expanded decidual tissue, and a disruption in
331 the structural organization of the two main placental compartments (junctional and labyrinth
332 zones). NK cells are known contributors to early events in uterine spiral artery remodeling

333 (Chakraborty *et al*, 2011; Erlebacher, 2013; Rätsep *et al*, 2015; Renaud *et al*, 2017). NK cells
334 vacate the uterine-placental interface as invasive trophoblast cells enter the uterus (Ain *et al*,
335 2003). In addition to PPARG, TFAP2C is also a driver of invasive trophoblast cell infiltration into
336 the uterus (Dominguez *et al*, 2024). Impairments of either PPARG or TFAP2C lead to failed
337 intrauterine trophoblast cell invasion and retention of NK cells within the uterine-placental
338 interface. The implication is that invasive trophoblast cells are engineering the exit of NK cells
339 from the uterine-placental interface. In the absence of invasive trophoblast cells, NK cells are
340 supporting, at least partially, uterine spiral artery remodeling and minimizing adverse pregnancy
341 outcomes. The nature of the signal(s) emanating from invasive trophoblast cells responsible for
342 NK cell exodus is unknown. Cooperation of invasive trophoblast cells and NK cells at the uterine-
343 placental interface is robust. It is expected that deficits in both maternal and extraembryonic
344 contributions to uterine transformation would exhibit more adverse consequences. Expansion of
345 the decidua compartment in *Pparg*$^{d/d}$ placentation sites could also be contributing to decreased
346 trophoblast cell migration towards the uterine-placental interface within the *Pparg*$^{d/d}$ placentation
347 sites. In addition to the uterine-placental interface, failure in the developmental progression of
348 progenitor cells situated in the junctional zone into invasive trophoblast cells resulted in
349 malformations within the junctional zone. These aberrations included the appearance of large
350 cystic structures within the junctional zone and an irregular junctional zone-labyrinth zone
351 interface. Specific cellular dysfunctions linked to PPARG deficiency underlying these structural
352 defects in junctional zone morphogenesis are unknown.
353
354 Finally, PPARG transcriptional activity is influenced by the availability of glucose and lipids
355 (Berger & Moller, 2002; Feige *et al*, 2006; Ahmadian *et al*, 2013). Thus, PPARG acts as a nutrient
356 sensor. Coupling nutrient sensing with the regulation of invasive trophoblast cell transformation of
357 the uterine vasculature would be an effective strategy for adapting to a nutrient-variable maternal
358 environment and is testable with the in vitro and in vivo models described in this report.
359
360 **Methods and Protocols**

361 *Human placentation site specimens*

362 Paraffin-embedded first-trimester placental tissue specimens were obtained from the
363 Lunenfeld-Tanenbaum Research Institute at Mount Sinai Hospital (Toronto, Canada). All tissue
364 samples were deidentified prior to use in this study. Tissue collection was conducted following
365 written informed consent and with approval from the Human Research Ethics Review Committees
366 at the University of Toronto and the University of Kansas Medical Center (**KUMC**).

367

368 *Human TS cell culture*

369 Human TS cells (CT27 and CT29) used in this study have been previously described (Okae
370 *et al*, 2018). The TS cells originated from deidentified first trimester human placental tissue
371 obtained from healthy women with signed informed consent and approval from the Ethics
372 Committee of Tohoku University School of Medicine. Experimentation with human TS cells was
373 approved by the KUMC Human Research Protection Program and the KUMC Human Stem Cell
374 Research Oversite committee. Human TS cell lines were maintained in the stem cell state and
375 differentiated into EVT cells as previously reported. Detailed culture conditions are provided in the
376 Appendix section.

377

378 *Design and generation of lentiviral shRNA constructs*

379 PPARG shRNA sequences were designed using the Genetic Perturbation Platform web
380 portal from the Broad Institute (https://portals.broadinstitute.org/gpp/public/analysis-tools/sgrna-
381 design), and subcloned into the pLKO.1 vector at *AgeI* and *EcoRI* restriction sites. An
382 shRNA control (**shCTRL**, Plasmid 1864, Addgene), which does not recognize any known
383 mammalian gene, was similarly subcloned into the pLKO.1 vector and used as a control. shRNA
384 sequences used in these analyses are listed in Appendix section Table 2. Lentiviral packaging
385 plasmids were obtained from Addgene and included pMDLg/pRRE (plasmid 12251), pRSV-Rev
386 (plasmid 12253), and pMD2.G (plasmid 12259). Lentiviral particles were produced via transient
387 transfection of the shRNA-pLKO.1 vector along with the packaging plasmids into Lenti-X cells
388 (632180, Takara Bio USA) using Attractene (301005, Qiagen) in Opti-MEM I (51985-034, Thermo

389 Fisher). Cells were maintained in Dulbecco's Modified Eagle Medium (DMEM, 11995-065,
390 Thermo Fisher) supplemented with 10% fetal bovine serum (**FBS**) for 24 h prior to supernatant
391 collection. At that point, cells were switched to Basal Human TS Cell Medium. Conditioned
392 medium containing viral particles was collected every 24 h over two days and stored at −80 °C
393 until used.
394
395 *Lentiviral transduction*
396 Human TS cells were plated at 65,000 cells per well in 6-well tissue culture-treated plates
397 coated with 5 µg/mL collagen IV (CB40233, Thermo Fisher) and incubated for 24 h. Prior to
398 transduction, medium was changed, and cells were incubated with 2.5 µg/mL polybrene for 30
399 min at 37°C. Following polybrene treatment, TS cells were transduced with 500 µL of conditioned
400 medium containing lentiviral particles and then incubated for 24 h. Medium was changed at 24 h
401 post transduction and selected with puromycin dihydrochloride (5 µg/mL, A11138-03, Thermo
402 Fisher) for 2 days. Cells recovered were cultured for 1 to 3 days in Complete TS Cell Medium and
403 then used to evaluate the effects of PPARG disruption on EVT cell differentiation.
404
405 *Cell migration assay*
406 Trophoblast cell migration was assessed according to the method described by Shimizu and
407 coworkers (Shimizu *et al*, 2023) with minor modifications. A suspension of 200,000 human TS
408 cells was prepared in Matrigel (100%) and Basal Human EVT Cell Differentiation Medium (10
409 µL). From this mixture, 1 µL was dispensed onto a 6-well plate to form individual Matrigel drops.
410 Six Matrigel drops were prepared. The drops were cultured in complete EVT cell differentiation
411 medium supplemented with 0.5% Matrigel (CB-40234, Thermo Fisher) at 37°C in a humidified
412 atmosphere containing 5% CO_2. Culture medium was replaced on day 3, and the cells were
413 incubated for a total of five days. EVT cells migrating from the cell aggregate were identified using
414 immunocytochemistry for HLA-G (1:300, phycoerythrin (**PE**)-labeled anti-HLA-G antibody,
415 ab24384, Abcam). After 15 min of incubation at 37°C, cells were fixed with 4% paraformaldehyde
416 (**PFA**). Nuclei were counterstained with 4',6-diamidino-2-phenylindole (**DAPI**, 1:50,000, D1306,

417 Invitrogen). Following washes with phosphate buffered saline (**PBS**, pH 7.4), the samples were
418 imaged using a Zeiss Axio Observer 7 microscope. The area of PE-labeled signal was quantified
419 using ImageJ software.
420
421 *Trophoblast organoids*
422 Human TS cells were used to establish trophoblast organoids as previously described
423 (Karvas *et al*, 2022) with minor modifications. Effects of PPARG on trophoblast organoid
424 formation and capacity to differentiate into EVT cells were determined. Detailed culture conditions
425 are provided in the Appendix section.
426
427 *Animals and tissue collection*
428 Holtzman Sprague–Dawley rats were obtained from Envigo and used for in vivo experiments.
429 Animals were housed in an environmentally controlled facility under a 14-hour light/10-hour dark
430 lighting schedule with food and water available ad libitum. Timed pregnancies were established
431 by mating virgin female rats (8–10 weeks of age) with adult male rats (>3 months of age). Mating
432 was confirmed by the presence of sperm in the vaginal lavage, with the day of sperm detection
433 considered gd 0.5. Pseudopregnant females were generated by mating with vasectomized males,
434 and the presence of a seminal plug was designated as day 0.5 of pseudopregnancy. Pregnant
435 rats were euthanized at different days during gestation. Some placentation sites were frozen
436 intact in dry ice–cooled heptane and stored at –80 °C for subsequent histological analysis, while
437 other placentation sites were dissected into uterine–placental interface, junctional zone, and
438 labyrinth zone compartments, as previously describe (Ain *et al*, 2006).
439
440 *Conditional Pparg mutant rat*
441 In vivo *Pparg* disruption in invasive trophoblast cells was achieved using the Cre-loxP
442 system. LoxP cassettes were inserted into introns flanking Exons 2 and 3 of the *Pparg* locus
443 using *CRISPR*/Cas9 mediated homologous recombination (Fig. 7, Appendix section Table 3).
444 *CRISPR*/Cas9 reagents and templates were electroporated into one-cell rat embryos using a

445 NEPA21 electroporator (Nepa Gene), and embryos subsequently transferred to pseudopregnant
446 rats. Offspring were screened for mutations via polymerase chain reaction (**PCR**), and successful
447 loxP site insertion was confirmed by DNA sequencing (GeneWiz). A founder mutant animal was
448 backcrossed with wild-type rats to assess germline transmission. A *Prl7b1-Cre* recombinase rat
449 model was used to specifically disrupt *Pparg* in invasive trophoblast cells (Iqbal *et al*, 2024).
450
451 Genotyping and sex chromosome determinations were performed as previously described
452 (Dhakal & Soares, 2017). Genomic DNA was extracted from tail-tip biopsies using the Red
453 Extract-N-Amp Tissue PCR Kit (XNAT-1000RXN, Sigma-Aldrich) and used for genotyping. Primer
454 sequences for detecting conditional mutations and determining sex chromosome composition are
455 provided (Appendix section Table 4).
456
457 *RT-qPCR*
458 Total RNA was isolated from tissues using TRIzol reagent (15596018, Thermo Fisher). One
459 µg of RNA was used to synthesize complementary DNA (**cDNA**) using the High-Capacity
460 Reverse Transcription Kit (4368814, Applied Biosystems), followed by a 1:10 dilution in nuclease-
461 free water. Quantitative PCR (**qPCR**) was performed using PowerSYBR Green PCR Master Mix
462 (4367659, Thermo Fisher) and transcript-specific primer sets (250 nM). Primer sequences are
463 provided in Appendix section, Tables 5 and 6. qPCR was conducted with a QuantStudio 5 Real-
464 Time PCR System (Thermo Fisher) using the following cycling conditions: an initial denaturation
465 step at 95 °C for 10 min, followed by 40 cycles of two-step PCR (95°C for 15 sec, 60°C for 1 min).
466 A dissociation curve was then generated with the following steps: 95°C for 15 sec, 60°C for 1
467 min, and a final at 95°C for 15 sec. Relative mRNA expression levels were calculated using the
468 ΔΔCt method. Glyceraldehyde 3-phosphate dehydrogenase (*Gapdh*) and RNA polymerase II
469 subunit A (*POLR2A*) were used as reference genes for rat and human samples, respectively.
470
471 *In situ hybridization*

472 In situ hybridization was performed using paraffin-embedded human placenta and frozen rat
473 placentation site tissue sections and the RNAscope® Multiplex Fluorescent Reagent Kit v2
474 (Advanced Cell Diagnostics) following the manufacturer's instructions. Custom-designed probes
475 were used to detect the following transcripts: human *PPARG* (441691, NM_138712.3, target
476 region: 699–1779), human *NOTUM* (430311, NM_178493.5, target region: 259–814), rat *Pparg*
477 (313251, NM_001145367.1, target region: 305–1932); rat *Krt8* (87304-C2, NM_199370.1, target
478 region: 134–1472), and rat *Prl7b1* (860181-C2, NM_153738.1, target region: 28–900). Nuclei
479 were visualized using DAPI (323108, Advanced Cell Diagnostics). Images were captured using a
480 Zeiss Axio Observer 7 microscope.
481
482 *Immunohistochemistry of placental tissues*
483 Formalin fixed paraffin-embedded human placental tissue sections and frozen rat
484 placentation site sections (10 µm thick) fixed in 4% paraformaldehyde were processed for
485 immunohistochemical analyses. Tissue sections were blocked with 10% goat serum (50062Z,
486 Thermo Fisher) and incubated overnight at 4°C with primary antibodies against vimentin (1:300,
487 sc-6260, Santa Cruz Biotechnology), pan-cytokeratin (1:100, F3418, Sigma-Aldrich), perforin
488 (1:300, TP251, Amsbio), or PPARG (human: 1:100, sc-7273, Santa Cruz Biotechnology; rat:
489 1:100, 2435S, Cell Signaling Technology). Immunostaining was visualized using fluorescence-
490 tagged secondary antibodies: Alexa Fluor 488-conjugated goat anti-mouse IgG (A11001, Thermo
491 Fisher) and Alexa Fluor 568-conjugated goat anti-rabbit IgG (A11011, Thermo Fisher). Sections
492 were counterstained with DAPI, mounted in Fluoromount-G (0100-01, Southern Biotech), and
493 imaged using a Nikon 90i upright microscope equipped with Photometrics CoolSNAP-ES
494 monochrome camera (Roper). Regions of the uterine–placental interface containing cytokeratin-
495 positive cells were quantified using ImageJ software, as previously described (Dominguez *et al*,
496 2024; Rosario *et al*, 2008).
497
498 *Immunohistochemistry of trophoblast organoids*

499 Organoids were recovered from Matrigel using Cell Recovery Solution (354253, Corning) and
500 dissociated by gentle pipetting. After 30 min incubation on ice, samples were centrifuged (600 xg,
501 5 min), washed with PBS, and fixed in 4% paraformaldehyde on ice for 30 min. Fixed organoids
502 were suspended in 20% sucrose solution and incubated at 4°C overnight. The sucrose solution
503 was subsequently replaced with 1 mL of warm gelatin/sucrose solution and incubated at 37°C for
504 15 min. Blocks of gelatin containing trophoblast organoids were froze for 1-2 min and stored at-
505 80°C until processed for cryosection. Sections were permeabilized in PBS containing 4% bovine
506 serum albumin and 0.5% Triton X-100. Primary antibodies to HLA-G (1:300, phycoerythrin (**PE**)-
507 labeled, ab24384, Abcam), CGB (1:500, ab9528, Abcam) and TP63 (1:500, ab124762, Abcam)
508 were incubated with tissue sections overnight at 4°C, followed by secondary antibody incubation.
509 Sections were counterstained with DAPI, mounted in Fluoromount-G (0100-01, Southern
510 Biotech), and imaged using a Nikon 90i upright microscope equipped with Photometrics
511 CoolSNAP-ES monochrome camera (Roper).
512
513 *Western blotting*
514 Human trophoblast cell lysates were processed using the radioimmunoprecipitation assay
515 lysis buffer (sc-24948A, Santa Cruz Biotechnology) and protein concentrations determined using
516 the DC Protein Assay Kit (5000112, Bio-Rad). Proteins (50 to 70 μg/lane) were separated by
517 sodium dodecyl sulfate polyacrylamide gel electrophoresis. Separated proteins were
518 electrophoretically transferred to polyvinylidene difluoride membranes (10600023, GE
519 Healthcare) for 1 h at 25 V on a semi-dry transfer apparatus (Bio-Rad). Membranes were
520 subsequently blocked with 5% milk for 1 h at room temperature, followed by incubation with
521 antibodies to PPARG (1:200, 2435S, Cell Signaling Technology or GAPDH (1:5,000, AM4300,
522 Invitrogen) in 5% milk overnight at 4°C. After primary antibody incubation, the membranes were
523 washed in Tris-buffered saline with Tween 20 (**TBS-T**) three times (10 min/wash) at room
524 temperature. The membranes were then incubated with anti-mouse immunoglobulin G
525 conjugated to horseradish peroxidase (**HRP**; 1:5000, 7076, Cell Signaling Technology) or anti-
526 rabbit immunoglobulin G conjugated to horseradish peroxidase (**HRP**; 1:5000, 5127, Cell

527 Signaling Technology) in 5% milk for 1 h at room temperature, washed in TBS-T three times (10
528 min/wash) at room temperature, immersed in Immobilon Crescendo Western HRP Substrate
529 (WBLUR0500, Sigma-Aldrich), and luminescence detected using Chemi Doc MP Imager (Bio-
530 Rad). The integrated densities of proteins separated by western blotting were quantified using
531 NIH ImageJ. PPARG protein intensities were normalized to GAPDH protein intensities. All
532 quantifications were performed on at least three independent biological replicates.
533
534 *RNA-seq analysis*
535 Transcript profiles were generated from control and PPARG shRNA treated human CT27 TS
536 cells following EVT cell differentiation. Three independent lentiviral transductions for each shRNA
537 were analyzed. RNA was isolated and integrity assessed using an Agilent 2100 Bioanalyzer.
538 cDNA libraries prepared with Illumina TruSeq RNA preparation kits according to the
539 manufacturer's instructions. Barcoded cDNA libraries were multiplexed onto a TruSeq paired-end
540 flow cell and sequenced (100-bp paired-end reads) with a TruSeq 200-cycle sequencing-by-
541 synthesis kit. Samples were sequenced on an Illumina NovaSeq platform at the KUMC Genome
542 Sequencing Facility. Reads from *.fastq files were mapped to the human reference genome
543 (GRCh37) using CLC Genomics Workbench 12.0 (Qiagen). Transcript abundance was expressed
544 as total reads, and a false discovery rate of 0.05 was used as a cutoff for significant differential
545 expression. Statistical significance was calculated by empirical analysis of digital gene expression
546 followed by Bonferroni's correction.
547
548 *ChIP-seq analysis*
549 PPARG ChIP was performed on human CT27 TS cells following EVT cell differentiation using
550 commercially available SimpleChIP® Enzymatic Chromatin Immunoprecipitation Kit (Magnetic
551 Beads, 9003, Cell Signaling Technology) and PPARG antibody (2435S, Cell Signaling
552 Technology). Three independent replicates were processed. The ChIP-seq library was
553 constructed using the Tecan Ovation Ultralow DNA System V2 (NuGEN Technologies, Redwood

City, CA) and sequenced on an Illumina NovaSeq platform. Details of data processing and analyses are presented in Supplemental Material.

Statistics

Statistical analyses were performed with GraphPad Prism 10.2.3 software. Statistical comparisons were evaluated using Student's *t* test or one-way analysis of variance with Dunnett's post hoc test. Statistical significance was determined as $P<0.05$.

Study approval

All protocols using rats were approved by the University of Kansas Medical Center Animal Care and Use Committee, Kansas City, Kansas (approved protocol 22-01-220).

Data availability

RNA-seq and ChIP-seq datasets are available at the Gene Expression Omnibus database, https://www.ncbi.nlm.nih.gov/geo/ (GSE302291 and GSE302293).

The source data of this paper are collected in the following database record, https://www.ebi.ac.uk/biostudies/bioimages/studies/S-BIAD2948

All data generated and analyzed in this study are included in the published article and supporting files.

Author Contributions

E.M.D and M.J.S. conceived and designed the research; E.M.D., A.M-I. and A.F. performed experiments; K.I., H.O., and T.A. provided experimental tools for analysis; E.M.D., A.M-I., K.C., G.T., M.P., and M.J.S. analyzed the data and interpreted results of experiments; E.M.D. and M.J.S. prepared the manuscript. All authors read, contributed to editing, and approved the final version of manuscript.

582

583 **Disclosure and Competing Interest Statement**

584 The authors have declared that no conflict of interest exists.

585

586 **Acknowledgments**

587 We thank Brandi Miller and Stacy Oxley for administrative assistance. The work was
588 supported by the Lalor Foundation (E.M.D., A.M.-I.), Kansas Idea Network of Biomedical
589 Research Excellence, P20 GM103418 (E.M.D, A.M.-I.), Program of the Joint Usage/Research
590 Center for Developmental Medicine and High Depth Omics, IMEG, Kumamoto University (H.O.),
591 NIH grants: HD115834 (A.M.-I.), HD104071 (K.I.), HD020676 (M.J.S.), HD105734 (M.J.S.),
592 HD112559 (M.J.S., G.T.), the Sosland Foundation (M.J.S.), and the Donald C. Johnson Research
593 Endowment Fund.

594

595 **References**

596 Ahmadian M, Suh JM, Hah N, Liddle C, Atkins AR, Downes M & Evans RM (2013) PPARγ signaling
597 and metabolism: the good, the bad and the future. *Nat Med* 19: 10.1038/nm.3159

598 Ain R, Canham LN & Soares MJ (2003) Gestation stage-dependent intrauterine trophoblast cell
599 invasion in the rat and mouse: novel endocrine phenotype and regulation. *Dev Biol* 260:
600 176–190

601 Ain R, Konno T, Canham LN & Soares MJ (2006) Phenotypic analysis of the rat placenta. *Methods*
602 *Mol Med* 121: 295–313

603 Asami-Miyagishi R, Iseki S, Usui M, Uchida K, Kubo H & Morita I (2004) Expression and function
604 of PPARgamma in rat placental development. *Biochem Biophys Res Commun* 315: 497–
605 501

606 Aye ILMH, Tong S, Charnock-Jones DS & Smith GCS (2025) The human placenta and its role in
607 reproductive outcomes revisited. *Physiol Rev* 105: 2305–2376

608 Barak Y, Nelson MC, Ong ES, Jones YZ, Ruiz-Lozano P, Chien KR, Koder A & Evans RM (1999)
609 PPAR gamma is required for placental, cardiac, and adipose tissue development. *Mol*
610 *Cell* 4: 585–595

611 Berger J & Moller DE (2002) The mechanisms of action of PPARs. *Annu Rev Med* 53: 409–435

612 Brosens I, Pijnenborg R, Vercruysse L & Romero R (2011) THE "GREAT OBSTETRICAL
613 SYNDROMES" ARE ASSOCIATED WITH DISORDERS OF DEEP PLACENTATION. *Am J Obstet*
614 *Gynecol* 204: 193–201

615 Brosens I, Puttemans P & Benagiano G (2019) Placental bed research: I. The placental bed:
616 from spiral arteries remodeling to the great obstetrical syndromes. *Am J Obstet Gynecol*
617 221: 437–456

618 Calkins K & Devaskar SU (2011) Fetal origins of adult disease. *Curr Probl Pediatr Adolesc Health*
619 *Care* 41: 158–176

620 Carter AM & Enders AC (2004) Comparative aspects of trophoblast development and
621 placentation. *Reprod Biol Endocrinol* 2: 46

622 Chakraborty D, Cui W, Rosario GX, Scott RL, Dhakal P, Renaud SJ, Tachibana M, Rumi MAK,
623 Mason CW, Krieg AJ, *et al* (2016) HIF-KDM3A-MMP12 regulatory circuit ensures
624 trophoblast plasticity and placental adaptations to hypoxia. *Proc Natl Acad Sci U S A*
625 113: E7212–E7221

626 Chakraborty D, Rumi MAK, Konno T & Soares MJ (2011) Natural killer cells direct hemochorial
627 placentation by regulating hypoxia-inducible factor dependent trophoblast lineage
628 decisions. *Proc Natl Acad Sci U S A* 108: 16295–16300

629 Chang W-L, Liu Y-W, Dang Y-L, Jiang X-X, Xu H, Huang X, Wang Y-L, Wang H, Zhu C, Xue L-Q, *et al*
630 (2018) PLAC8, a new marker for human interstitial extravillous trophoblast cells,
631 promotes their invasion and migration. *Development* 145: dev148932

632 Dhakal P & Soares MJ (2017) Single Step PCR-Based Genetic Sex Determination for Rat Tissues
633 and Cells. *Biotechniques* 62: 232–233

634 Dominguez EM, Moreno-Irusta A, Scott RL, Iqbal K & Soares MJ TFAP2C is a key regulator of
635 intrauterine trophoblast cell invasion and deep hemochorial placentation. *JCI Insight* 10:
636 e186471

637 Erlebacher A (2013) Immunology of the maternal-fetal interface. *Annu Rev Immunol* 31: 387–
638 411

639 Feige JN, Gelman L, Michalik L, Desvergne B & Wahli W (2006) From molecular action to
640 physiological outputs: peroxisome proliferator-activated receptors are nuclear receptors
641 at the crossroads of key cellular functions. *Prog Lipid Res* 45: 120–159

642 Fisher SJ (2015) Why is placentation abnormal in preeclampsia? *Am J Obstet Gynecol* 213: S115–
643 S122

644 Fournier T, Guibourdenche J, Handschuh K, Tsatsaris V, Rauwel B, Davrinche C & Evain-Brion D
645 (2011) PPARγ and human trophoblast differentiation. *J Reprod Immunol* 90: 41–49

646 Fournier T, Tsatsaris V, Handschuh K & Evain-Brion D (2007) PPARs and the placenta. *Placenta*
647 28: 65–76

648 Georgiades P, Ferguson-Smith AC & Burton GJ (2002) Comparative developmental anatomy of
649 the murine and human definitive placentae. *Placenta* 23: 3–19

650 Gluckman PD, Hanson MA, Cooper C & Thornburg KL (2008) Effect of In Utero and Early-Life
651 Conditions on Adult Health and Disease. *N Engl J Med* 359: 61–73

652 Guo Q, Choi J, Lee M & Kim J (2025) PPARG-centric transcriptional re-wiring during
653 differentiation of human trophoblast stem cells into extravillous trophoblasts. *Nucleic*
654 *Acids Res* 53: gkaf669

655 Harris LK (2010) Review: Trophoblast-vascular cell interactions in early pregnancy: how to
656 remodel a vessel. *Placenta* 31 Suppl: S93-98

657 Harris LK, Benagiano M, D'Elios MM, Brosens I & Benagiano G (2019) Placental bed research: II.
658 Functional and immunological investigations of the placental bed. *Am J Obstet Gynecol*
659 221: 457–469

660 Hemberger M, Nozaki T, Masutani M & Cross JC (2003) Differential expression of angiogenic and
661 vasodilatory factors by invasive trophoblast giant cells depending on depth of invasion.
662 *Dev Dyn* 227: 185–191

663 Holdsworth-Carson SJ, Lim R, Mitton A, Whitehead C, Rice GE, Permezel M & Lappas M (2010)
664 Peroxisome proliferator-activated receptors are altered in pathologies of the human
665 placenta: gestational diabetes mellitus, intrauterine growth restriction and
666 preeclampsia. *Placenta* 31: 222–229

667 Iqbal K, Dominguez EM, Nixon B, Moreno-Irusta A, Crnkovich B, Scott RL, Vu HTH, Tuteja G,
668 Vivian JL & Soares MJ (2024) Conditionally mutant animal model for investigating the
669 invasive trophoblast cell lineage. *Development* 151: dev202239

670 Jeyarajah MJ, Jaju Bhattad G, Kelly RD, Baines KJ, Jaremek A, Yang F-HP, Okae H, Arima T,
671 Dumeaux V & Renaud SJ The multifaceted role of GCM1 during trophoblast
672 differentiation in the human placenta. *Proc Natl Acad Sci U S A* 119: e2203071119

673 Kadam L, Kohan-Ghadr HR & Drewlo S (2015) The balancing act – PPAR-γ's roles at the maternal-
674 fetal interface. *Syst Biol Reprod Med* 61: 65–71

675 Karvas RM, Khan SA, Verma S, Yin Y, Kulkarni D, Dong C, Park K, Chew B, Sane E, Fischer LA, *et al*
676 (2022) Stem-cell-derived trophoblast organoids model human placental development
677 and susceptibility to emerging pathogens. *Cell Stem Cell* 29: 810-825.e8

678 Kaufmann P, Black S & Huppertz B (2003) Endovascular trophoblast invasion: implications for
679 the pathogenesis of intrauterine growth retardation and preeclampsia. *Biol Reprod* 69:
680 1–7

681 Kim M, Jang YJ, Lee M, Guo Q, Son AJ, Kakkad NA, Roland AB, Lee B-K & Kim J (2024) The
682 transcriptional regulatory network modulating human trophoblast stem cells to
683 extravillous trophoblast differentiation. *Nat Commun* 15: 1285

684 Kubota N, Terauchi Y, Miki H, Tamemoto H, Yamauchi T, Komeda K, Satoh S, Nakano R, Ishii C,
685 Sugiyama T, *et al* (1999) PPAR gamma mediates high-fat diet-induced adipocyte
686 hypertrophy and insulin resistance. *Mol Cell* 4: 597–609

687 Kuna M, Dhakal P, Iqbal K, Dominguez EM, Kent LN, Muto M, Moreno-Irusta A, Kozai K, Varberg
688 KM, Okae H, *et al* CITED2 is a conserved regulator of the uterine–placental interface.
689 *Proc Natl Acad Sci U S A* 120: e2213622120

690 Liu Y, Fan X, Wang R, Lu X, Dang Y-L, Wang H, Lin H-Y, Zhu C, Ge H, Cross JC, *et al* (2018) Single-
691 cell RNA-seq reveals the diversity of trophoblast subtypes and patterns of differentiation
692 in the human placenta. *Cell Res* 28: 819–832

693 Maltepe E & Fisher SJ (2015) Placenta: the forgotten organ. *Annu Rev Cell Dev Biol* 31: 523–552

694 Meinhardt G, Waldhäusl H, Lackner AI, Wächter J, Maxian T, Höbler A-L, Vondra S, Kunihs V,
695 Saleh L, Haslinger P, *et al* The multifaceted roles of the transcriptional coactivator TAZ in
696 extravillous trophoblast development of the human placenta. *Proc Natl Acad Sci U S A*
697 122: e2426385122

698 Muto M, Chakraborty D, Varberg KM, Moreno-Irusta A, Iqbal K, Scott RL, McNally RP, Choudhury
699 RH, Aplin JD, Okae H, *et al* (2021) Intersection of regulatory pathways controlling
700 hemostasis and hemochorial placentation. *Proc Natl Acad Sci U S A* 118: e2111267118

701 Okae H, Toh H, Sato T, Hiura H, Takahashi S, Shirane K, Kabayama Y, Suyama M, Sasaki H &
702 Arima T (2018) Derivation of Human Trophoblast Stem Cells. *Cell Stem Cell* 22: 50-63.e6

703 Parast MM, Yu H, Ciric A, Salata MW, Davis V & Milstone DS (2009) PPARγ Regulates Trophoblast
704 Proliferation and Promotes Labyrinthine Trilineage Differentiation. *PLoS ONE* 4: e8055

705 Pavan L, Tarrade A, Hermouet A, Delouis C, Titeux M, Vidaud M, Thérond P, Evain-Brion D &
706 Fournier T (2003) Human invasive trophoblasts transformed with simian virus 40
707 provide a new tool to study the role of PPARγ in cell invasion process. *Carcinogenesis* 24:
708 1325–1336

709 Pijnenborg R, Robertson WB, Brosens I & Dixon G (1981) Review article: trophoblast invasion
710 and the establishment of haemochorial placentation in man and laboratory animals.
711 *Placenta* 2: 71–91

712 Pijnenborg R, Vercruysse L & Hanssens M (2006) The uterine spiral arteries in human pregnancy:
713 facts and controversies. *Placenta* 27: 939–958

714 Rai A & Cross JC (2014) Development of the hemochorial maternal vascular spaces in the
715 placenta through endothelial and vasculogenic mimicry. *Dev Biol* 387: 131–141

716 Rätsep MT, Felker AM, Kay VR, Tolusso L, Hofmann AP & Croy BA (2015) Uterine natural killer
717 cells: supervisors of vasculature construction in early decidua basalis. *Reproduction* 149:
718 R91-102

719 Renaud SJ, Scott RL, Chakraborty D, Rumi MAK & Soares MJ (2017) Natural killer-cell deficiency
720 alters placental development in rats. *Biol Reprod* 96: 145–158

721 Roberts RM, Green JA & Schulz LC (2016) The evolution of the placenta. *Reproduction* 152:
722 R179-189

723 Rodie VA, Young A, Jordan F, Sattar N, Greer IA & Freeman DJ (2005) Human placental
724 peroxisome proliferator-activated receptor delta and gamma expression in healthy
725 pregnancy and in preeclampsia and intrauterine growth restriction. *J Soc Gynecol*
726 *Investig* 12: 320–329

727 Rosario GX, Konno T & Soares MJ (2008) Maternal hypoxia activates endovascular trophoblast
728 cell invasion. *Dev Biol* 314: 362–375

729 Sauer S (2015) Ligands for the Nuclear Peroxisome Proliferator-Activated Receptor Gamma.
730 *Trends Pharmacol Sci* 36: 688–704

731 Schaiff WT, Barak Y & Sadovsky Y (2006) The pleiotropic function of PPARγ in the placenta.
732 *Molecular and Cellular Endocrinology* 249: 10–15

733 Schaiff WT, Bildirici I, Cheong M, Chern PL, Nelson DM & Sadovsky Y (2005) Peroxisome
734 proliferator-activated receptor-gamma and retinoid X receptor signaling regulate fatty
735 acid uptake by primary human placental trophoblasts. *J Clin Endocrinol Metab* 90: 4267–
736 4275

737 Schaiff WT, Carlson MG, Smith SD, Levy R, Nelson DM & Sadovsky Y (2000) Peroxisome
738 proliferator-activated receptor-gamma modulates differentiation of human trophoblast
739 in a ligand-specific manner. *J Clin Endocrinol Metab* 85: 3874–3881

740 Scott RL, Vu HTH, Jain A, Iqbal K, Tuteja G & Soares MJ (2022) Conservation at the uterine–
741 placental interface. *Proceedings of the National Academy of Sciences* 119: e2210633119

742 Shalom-Barak T, Nicholas JM, Wang Y, Zhang X, Ong ES, Young TH, Gendler SJ, Evans RM & Barak
743 Y (2004) Peroxisome proliferator-activated receptor gamma controls Muc1 transcription
744 in trophoblasts. *Mol Cell Biol* 24: 10661–10669

745 Shimizu T, Oike A, Kobayashi EH, Sekiya A, Kobayashi N, Shibata S, Hamada H, Saito M, Yaegashi
746 N, Suyama M, *et al* (2023) CRISPR screening in human trophoblast stem cells reveals
747 both shared and distinct aspects of human and mouse placental development.
748 *Proceedings of the National Academy of Sciences* 120: e2311372120

749 Shukla V, Moreno-Irusta A, Varberg KM, Kuna M, Iqbal K, Galligos AM, Aplin JD, Choudhury RH,
750 Okae H, Arima T, *et al* (2024) NOTUM-mediated WNT silencing drives extravillous
751 trophoblast cell lineage development. *Proc Natl Acad Sci U S A* 121: e2403003121

752 Shukla V & Soares MJ (2022) Modeling Trophoblast Cell-Guided Uterine Spiral Artery
753 Transformation in the Rat. *Int J Mol Sci* 23: 2947

754 Soares MJ, Chakraborty D, Karim Rumi MA, Konno T & Renaud SJ (2012) Rat placentation: an
755 experimental model for investigating the hemochorial maternal-fetal interface. *Placenta*
756 33: 233–243

757 Soares MJ, Varberg KM & Iqbal K (2018) Hemochorial placentation: development, function, and
758 adaptations. *Biol Reprod* 99: 196–211

759 Tarrade A (2001) PPAR /RXR Heterodimers Control Human Trophoblast Invasion. *Journal of*
760 *Clinical Endocrinology & Metabolism* 86: 5017–5024

761 Tarrade A, Schoonjans K, Guibourdenche J, Bidart JM, Vidaud M, Auwerx J, Rochette-Egly C &
762 Evain-Brion D (2001) PPARγ/RXRα Heterodimers Are Involved in Human CGβ Synthesis
763 and Human Trophoblast Differentiation. *Endocrinology* 142: 4504–4514

764 Varberg KM, Dominguez EM, Koseva B, Varberg JM, McNally RP, Moreno-Irusta A, Wesley ER,
765 Iqbal K, Cheung WA, Schwendinger-Schreck C, *et al* (2023) Extravillous trophoblast cell
766 lineage development is associated with active remodeling of the chromatin landscape.
767 *Nat Commun* 14: 4826

768 Varberg KM, Iqbal K, Muto M, Simon ME, Scott RL, Kozai K, Choudhury RH, Aplin JD, Biswell R,
769 Gibson M, *et al* (2021) ASCL2 reciprocally controls key trophoblast lineage decisions
770 during hemochorial placenta development. *Proc Natl Acad Sci U S A* 118: e2016517118

771 Velicky P, Knöfler M & Pollheimer J (2015) Function and control of human invasive trophoblast
772 subtypes: Intrinsic vs. maternal control. *Cell Adh Migr* 10: 154–162

773 Vento-Tormo R, Efremova M, Botting RA, Turco MY, Vento-Tormo M, Meyer KB, Park J-E,
774 Stephenson E, Polański K, Goncalves A, *et al* (2018) Single-cell reconstruction of the
775 early maternal-fetal interface in humans. *Nature* 563: 347–353

776 Vu HTH, Scott RL, Iqbal K, Soares MJ & Tuteja G (2023) Core conserved transcriptional regulatory
777 networks define the invasive trophoblast cell lineage. *Development* 150: dev201826

778 Waite LL, Louie RE & Taylor RN (2005) Circulating Activators of Peroxisome Proliferator-
779 Activated Receptors Are Reduced in Preeclamptic Pregnancy. *The Journal of Clinical*
780 *Endocrinology & Metabolism* 90: 620–626

781 Waite LL, Person EC, Zhou Y, Lim KH, Scanlan TS & Taylor RN (2000) Placental peroxisome
782 proliferator-activated receptor-gamma is up-regulated by pregnancy serum. *J Clin*
783 *Endocrinol Metab* 85: 3808–3814

784 Wang L-J, Chen C-P, Lee Y-S, Ng P-S, Chang G-D, Pao Y-H, Lo H-F, Peng C-H, Cheong M-L & Chen
785 H (2022) Functional antagonism between ΔNp63α and GCM1 regulates human
786 trophoblast stemness and differentiation. *Nat Commun* 13: 1626

787 Wiemers DO, Ain R, Ohboshi S & Soares MJ (2003) Migratory trophoblast cells express a newly
788 identified member of the prolactin gene family. *J Endocrinol* 179: 335–346

789 Xie J, Xu Y, Wan L, Wang P, Wang M & Dong M (2018) Involvement of follistatin-like 3 in
790 preeclampsia. *Biochem Biophys Res Commun* 506: 692–697

791

792

793 **Figures**

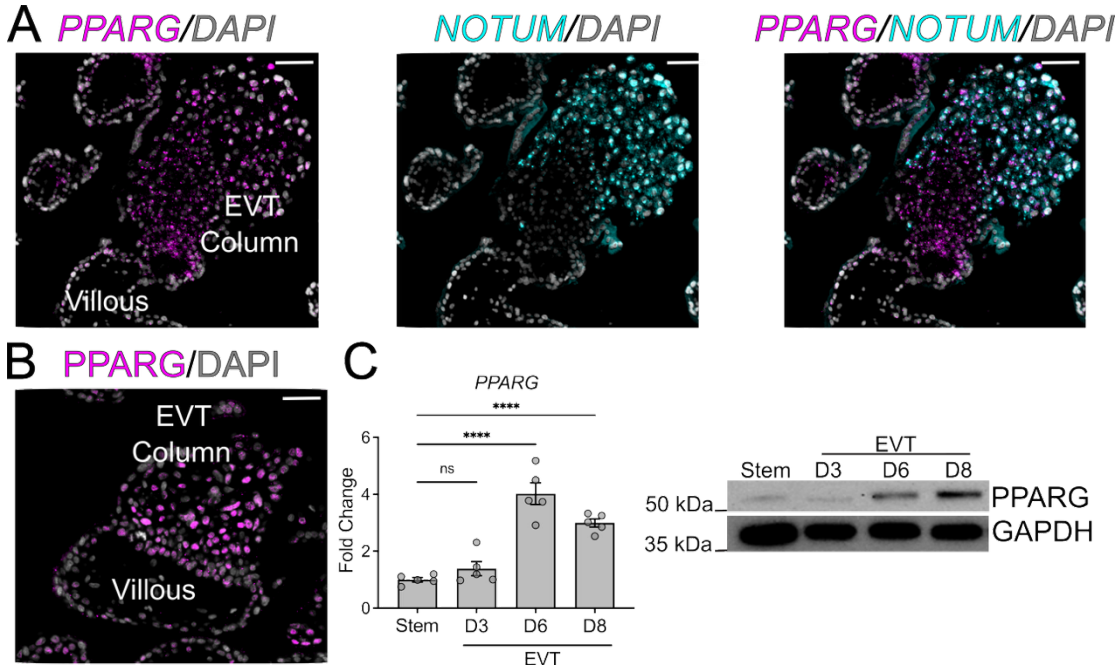

794

795 **Figure 1. PPARG is expressed in EVT cells. (A)** *PPARG* transcript (magenta) was localized
796 throughout the EVT column in first trimester human placenta (12 weeks) using in situ
797 hybridization. *NOTUM* (cyan) was used as a distal EVT cell specific transcript. **(B)** PPARG
798 immunohistochemistry (magenta) showed nuclear localization within cells of the first trimester
799 EVT cell column (12 weeks). Scale bars for panels A and B=500 μm. **(C)** In vitro *PPARG*
800 transcript and protein expression in CT27 (X,X) TS cells in the stem state, day 3 (D3), day 6 (D6),
801 and day 8 (D8) of EVT cell differentiation (n=5). Data are presented as mean ± standard error of
802 the mean. Each data point represents a biological replicate. Statistical analysis was performed
803 using ANOVA followed by Dunnett's post hoc test: ****p<0.0001.

804

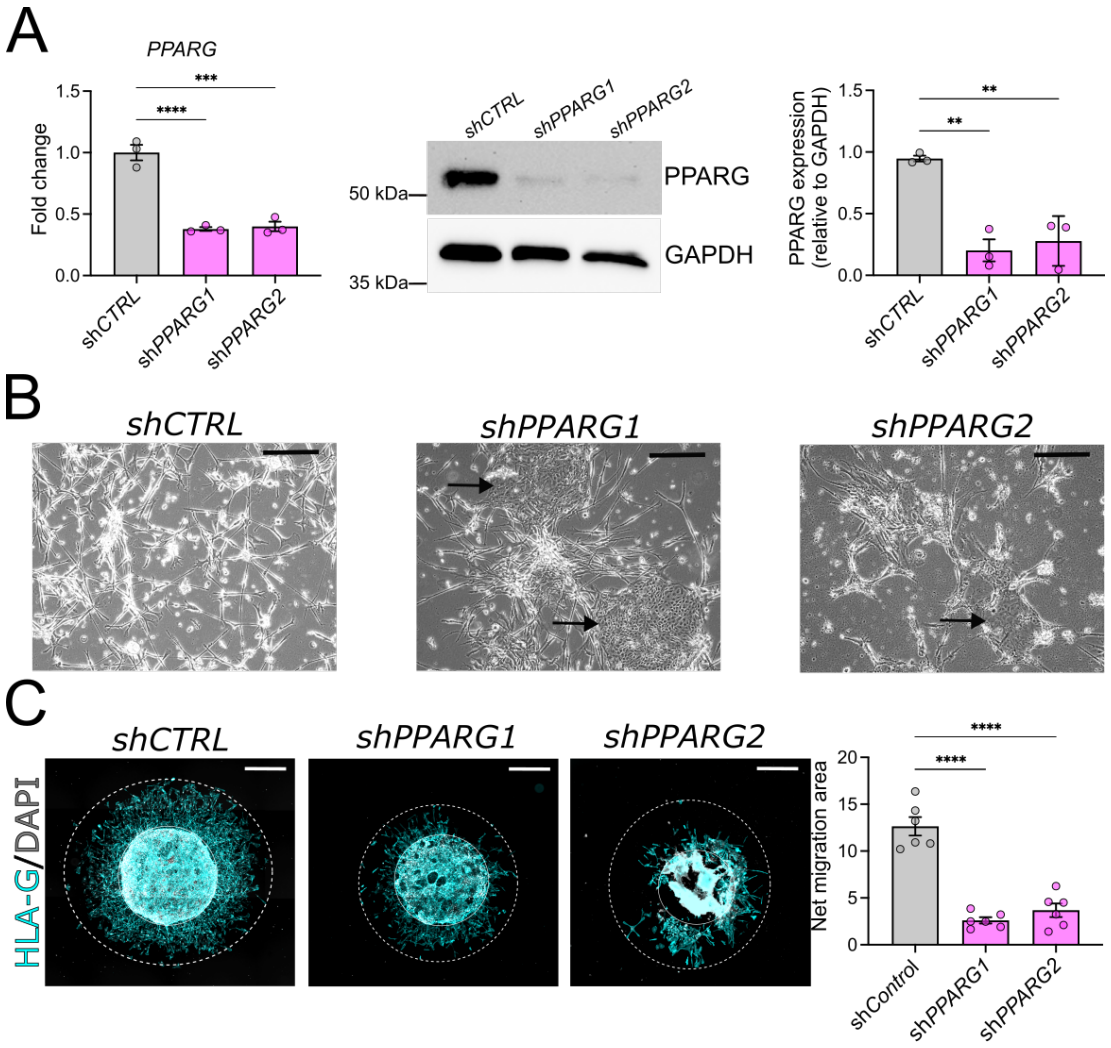

Figure 2. PPARG regulates EVT cell differentiation. (A) In vitro *PPARG* transcript and protein levels after 8 days of EVT cell differentiation in control versus PPARG1 and PPARG2 shRNAs-treated cells (n=3). **(B)** Phase-contrast images showing the morphology of EVT cells expressing control or PPARG1 and PPARG2 shRNAs. The arrow indicates a cluster of cells exhibiting a stem-like morphology, scale bar=100 µm. **(C)** HLA-G immunofluorescence detection of cell migration in control versus PPARG1 and PPARG2 shRNA-treated cells (n=6), scale bar=500 µm. Data are presented as the mean ± standard error of the mean. Each data point represents a biological replicate. Statistical analysis was performed using one-way ANOVA followed by Dunnett's post hoc tests: ** $p<0.01$, ***$p<0.001$, ****$p<0.0001$.

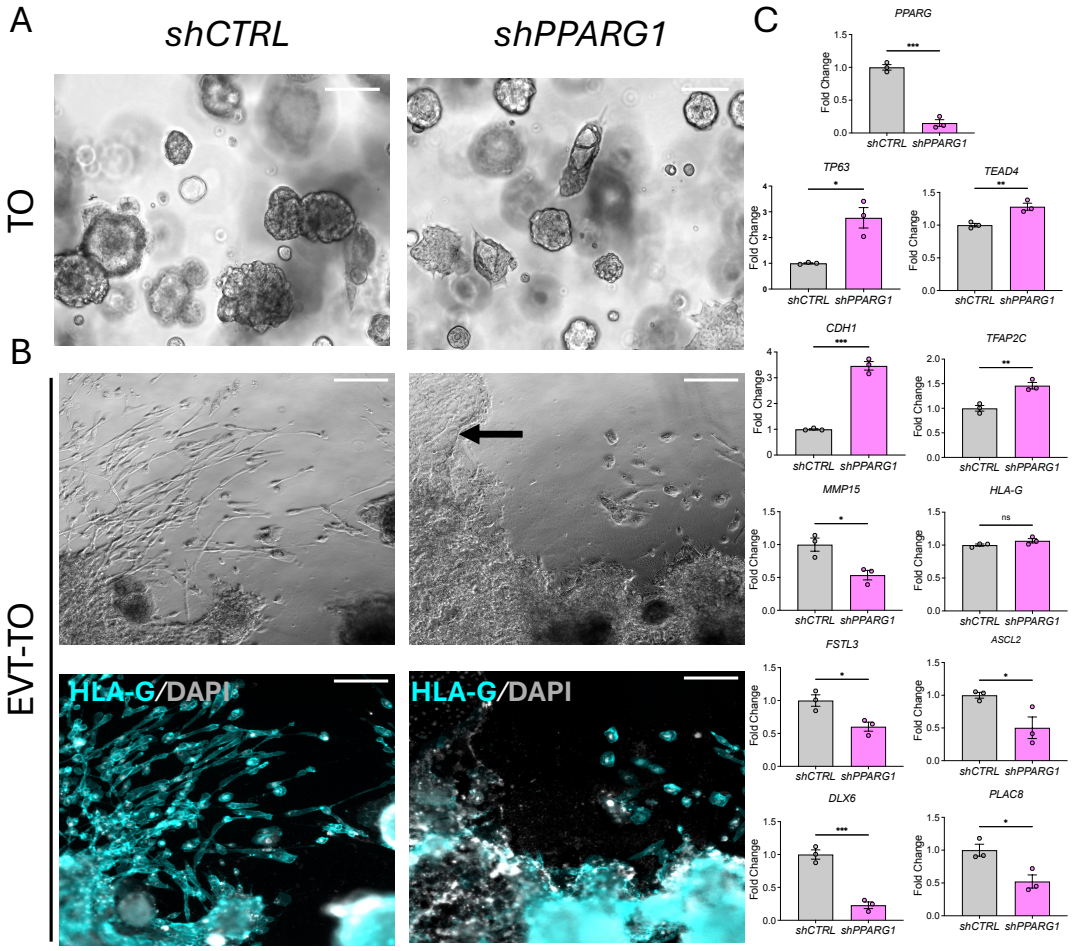

Figure 3. Examination of the role of PPARG in EVT cell differentiation using trophoblast organoids. **(A)** Phase-contrast images of trophoblast organoids (**TO**) expressing control (**shCTRL**) and PPARG (**shPPARG**) shRNAs, scale bar=100 µm. **(B)** Phase-contrast (top panel) and HLA-G immunostaining (bottom panel) images of shCTRL and shPPARG TO transferred to EVT cell differentiation conditions (**EVT-TO**). Arrows indicate the location of cells exhibiting stem-like morphology, scale bar=100 µm. **(C)** RT-qPCR analysis of shCTRL and shPPARG TO exposed to EVT cell differentiation conditions. Data are presented as the mean ± standard error of the mean. Each data point represents a biological replicate. Statistical analysis was performed using unpaired t-tests: *P<0.05, **p<0.01, ***p<0.001.

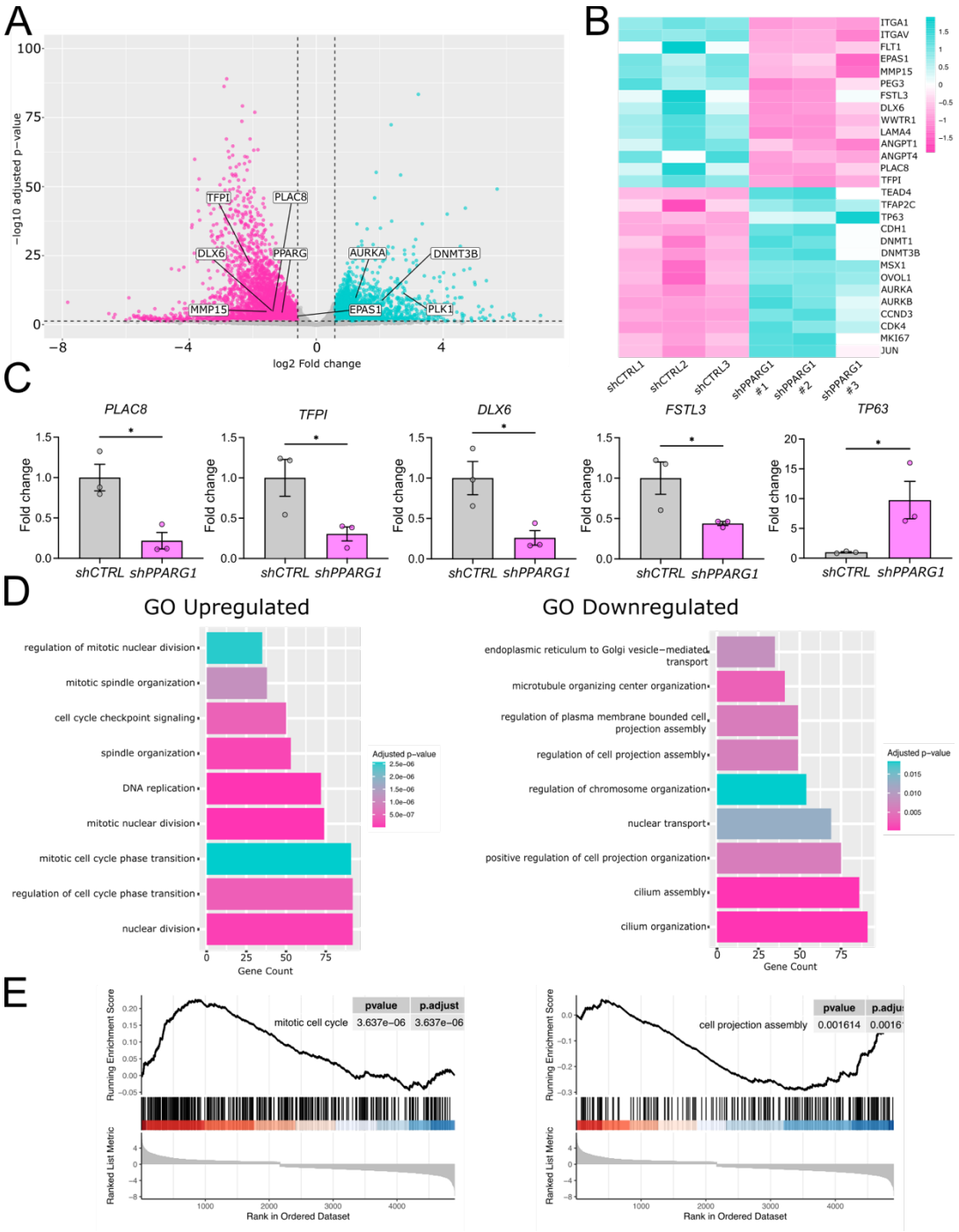

Figure 4. Effects of PPARG on the EVT cell transcriptome. (A) Volcano plot and **(B)** heat map depicting RNA-seq analysis of control shRNA and PPARG shRNA for cells exposed to culture conditions used to promote EVT cell differentiation (n=3 per group). Downregulated transcripts are represented by magenta dots ($p<0.05$, fold change <1.5) and cyan dots represent upregulated transcripts ($p<0.05$, fold change>1.5). Z-scores of totals read values are represented

833 in the heat map. **(C)** RT-qPCR validation of putative PPARG targets in control and PPARG
834 shRNA treated cells. **(D)** Gene ontology (GO) analyses of upregulated and downregulated genes
835 in control and PPARG shRNA treated TS cells exposed to culture conditions used to promote
836 EVT cell differentiation. **(E)** Gene set enrichment analyses of upregulated and downregulated
837 genes in control and PPARG shRNA treated TS cells exposed to culture conditions used to
838 promote EVT cell differentiation. CT27 (X,X) TS cell line was used for all experiments shown.
839 Data are presented as the mean ± standard error of the mean. Each data point represents a
840 biological replicate. Statistical analyses were performed using unpaired t-tests: *$p<0.05$.
841

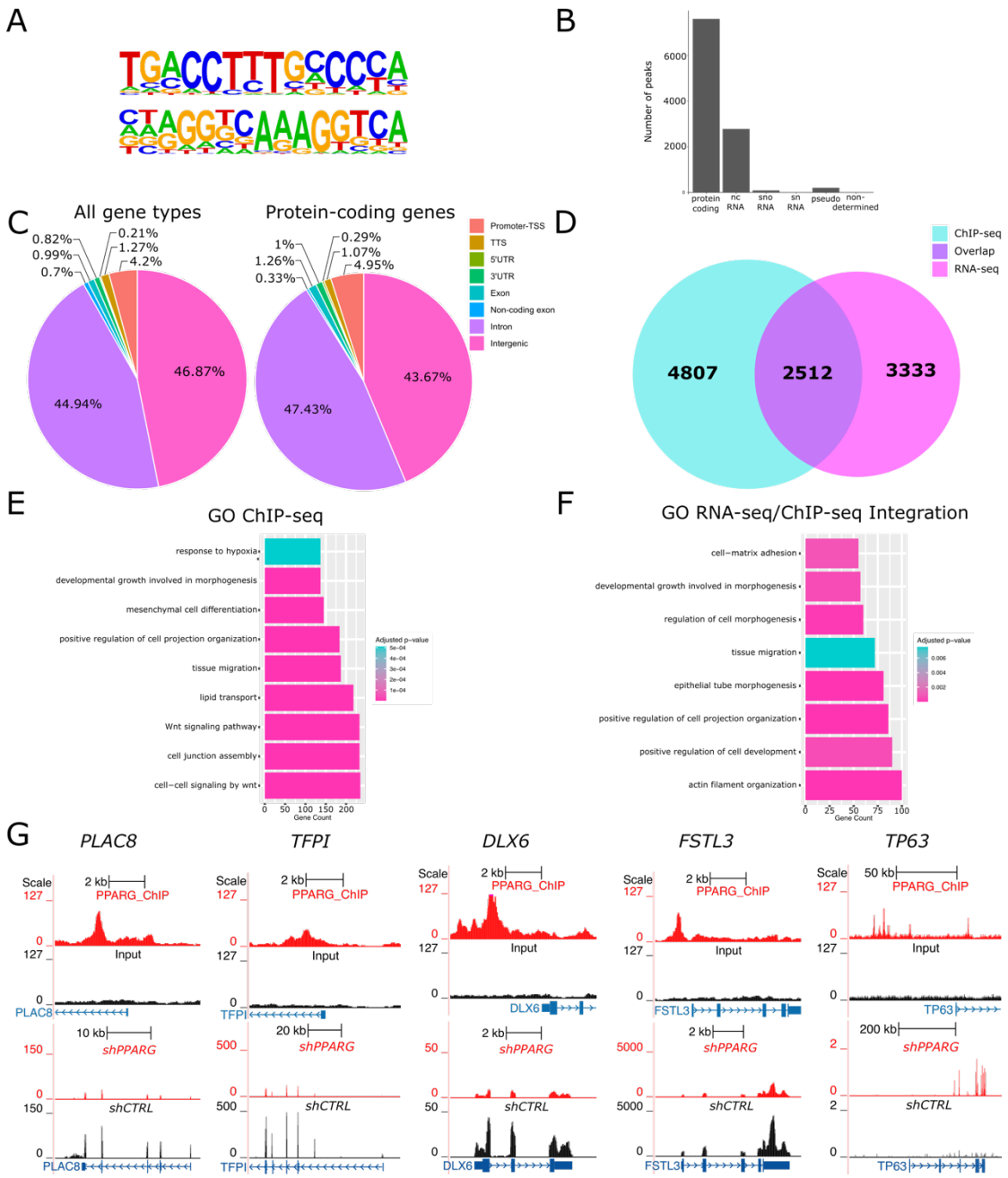

Figure 5. PPARG targets within the EVT cell genome identified using ChIP-seq. (A) Two significantly enriched PPARG binding motifs were observed within PPARG ChIP-seq peaks. **(B)** Number of peaks observed within specific locations of the genome. **(C)** Pie chart showing the distribution of PPARG peaks in genomic regions for all genes and protein-coding genes. **(D)** Venn diagram showing the integration of PPARG responsive genes identified by RNA-seq of EVT cells (**see Fig. 4**) and PPARG gene targets identified by PPARG ChIP-seq from EVT cells. **(E)** Gene ontology (**GO**) analysis of the PPARG ChIP-seq dataset performed on EVT cells. **(F)** GO analysis

850 of an integrated dataset generated from PPARG responsive genes identified by RNA-seq of EVT
851 cells (**see Fig. 4**) and PPARG gene targets identified by PPARG ChIP-seq from EVT cells. **(G)**
852 Integration of PPARG ChIP-Seq peaks and RNA-seq track at selected gene loci that exhibit
853 sensitivity to PPARG inhibition. Visualization was performed using the University of California at
854 Santa Cruz Genome browser. Red peaks represent PPARGbound regions in the ChIP-seq and
855 gene expression in shPPARG1 RNA-seq, whereas black peaks represent input DNA in ChIP-seq
856 and gene expression in shCTRL RNA-seq.
857

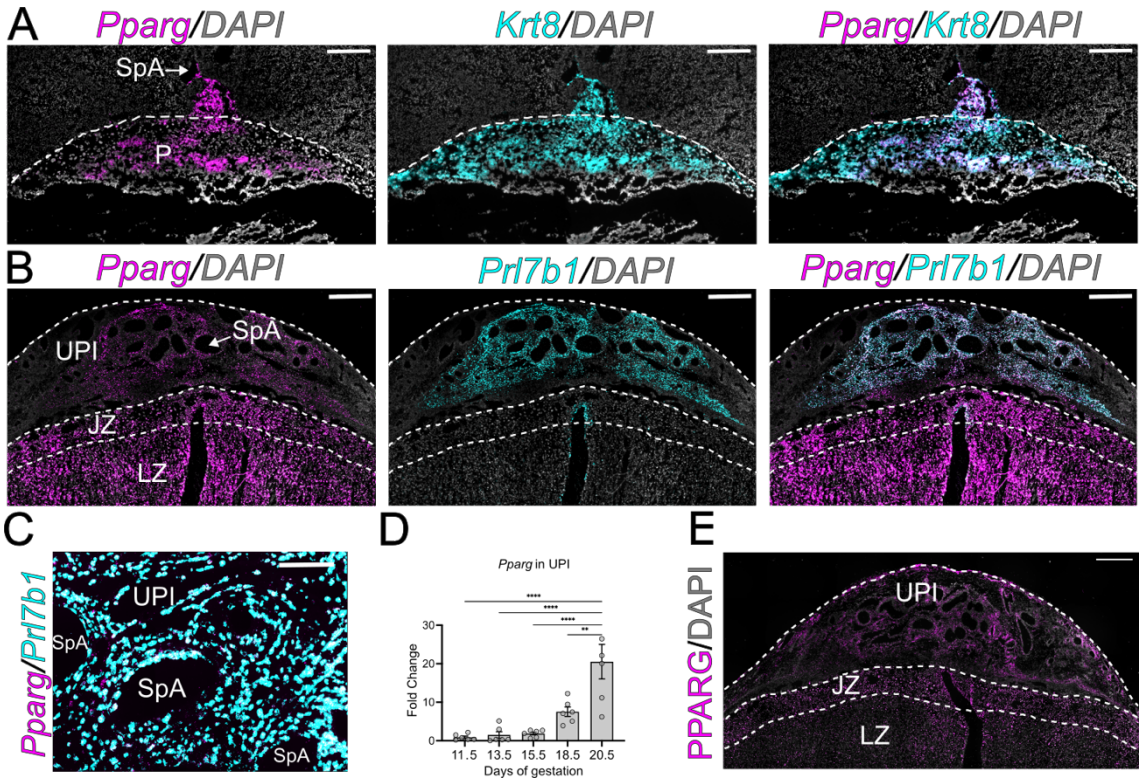

Figure 6. Distribution of *Pparg* transcripts and protein in rat placental tissues. *Pparg* transcripts were localized within rat placentation sites using in situ hybridization. **(A)** *Pparg* transcripts (magenta) were co-localized with *Krt8* transcripts (cyan) at gestation day (**gd**) 11.5. **(B)** Co-localization (white) of *Pparg* (magenta) and *Prl7b1* (cyan) transcripts within the gd 18.5 placentation site. **(C)** Higher magnification of the placentation site surrounding the spiral arteries showing co-localization (white) of *Pparg* (magenta) and *Prl7b1* (cyan) transcripts. **(D)** RT-qPCR measurement of *Pparg* transcript levels in uterine-placental interface tissues at gd 11.5, 13.5, 15.5, 18.5, and 20.5. Data are presented as mean ± standard error of the mean. Each data point represents a biological replicate from six independent pregnancies (n=6). Statistical analyses were performed with unpaired *t*-tests: **p<0.01, ****p<0.0001. **(E)** Immunohistochemical localization of PPARG protein within the gd 18.5 rat uterine-placental interface. Scale bars for panels A, B and E=500 µm, and panel C=50 µm. Abbreviations: SpA, spiral artery; UPI, uterine-placental interface; P, placenta; JZ, junctional zone; LZ, labyrinth zone.

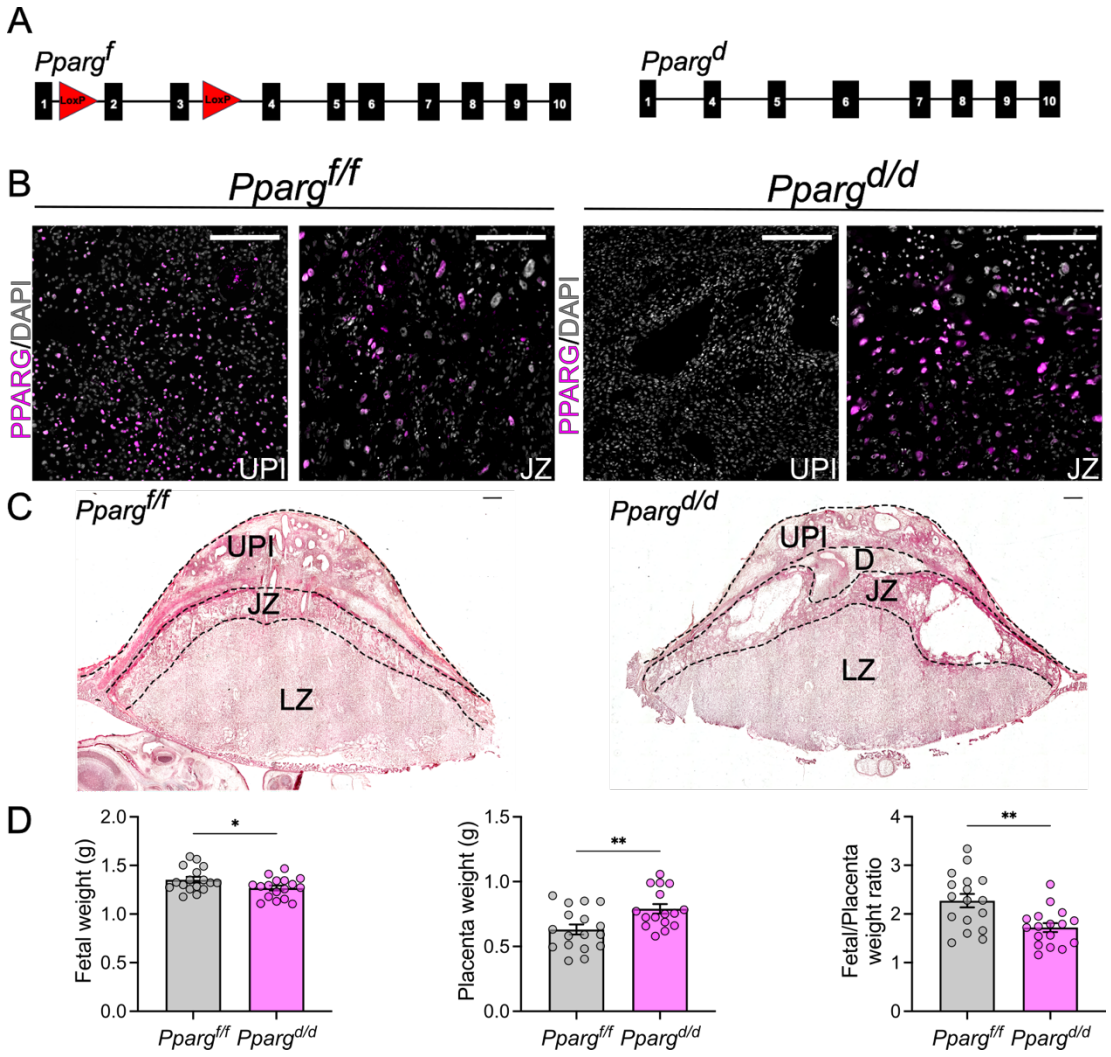

Figure 7. Rat invasive trophoblast-specific deletion of *Pparg*. (A) Schematic representation of loxP sites flanking Exons 2 and 3 of the *Pparg* gene and their conditional deletion following Cre recombinase activity driven by *Prl7b1* regulatory DNA. **(B)** PPARG immunostaining of *Pparg*$^{f/f}$ and *Pparg*$^{d/d}$ gestation day (**gd**) 18.5 placentation sites. Images show uterine-placental interface tissues (left) and junctional zone tissues (right) for each group, scale bar=50 µm. **(C)** Hematoxylin and eosin staining of *Pparg*$^{f/f}$ and *Pparg*$^{d/d}$ gd 18.5 placentation sites, scale bar=500 µm. **(D)** Placental weight, fetal weight, and fetal-to-placental weight ratio from gd 18.5 *Pparg*$^{f/f}$ and *Pparg*$^{d/d}$ conceptuses. Data are presented as mean ± standard error of the mean. Each data point represents a biological replicate from six pregnancies (*Pparg*$^{f/f}$, n=17, *Pparg*$^{d/d}$, n=17). Statistical analyses were performed using unpaired *t*-tests: *p<0.05, **p<0.01. Abbreviations: SpA, spiral artery; UPI, uterine-placental interface; JZ, junctional zone; LZ, labyrinth zone; D, decidua.

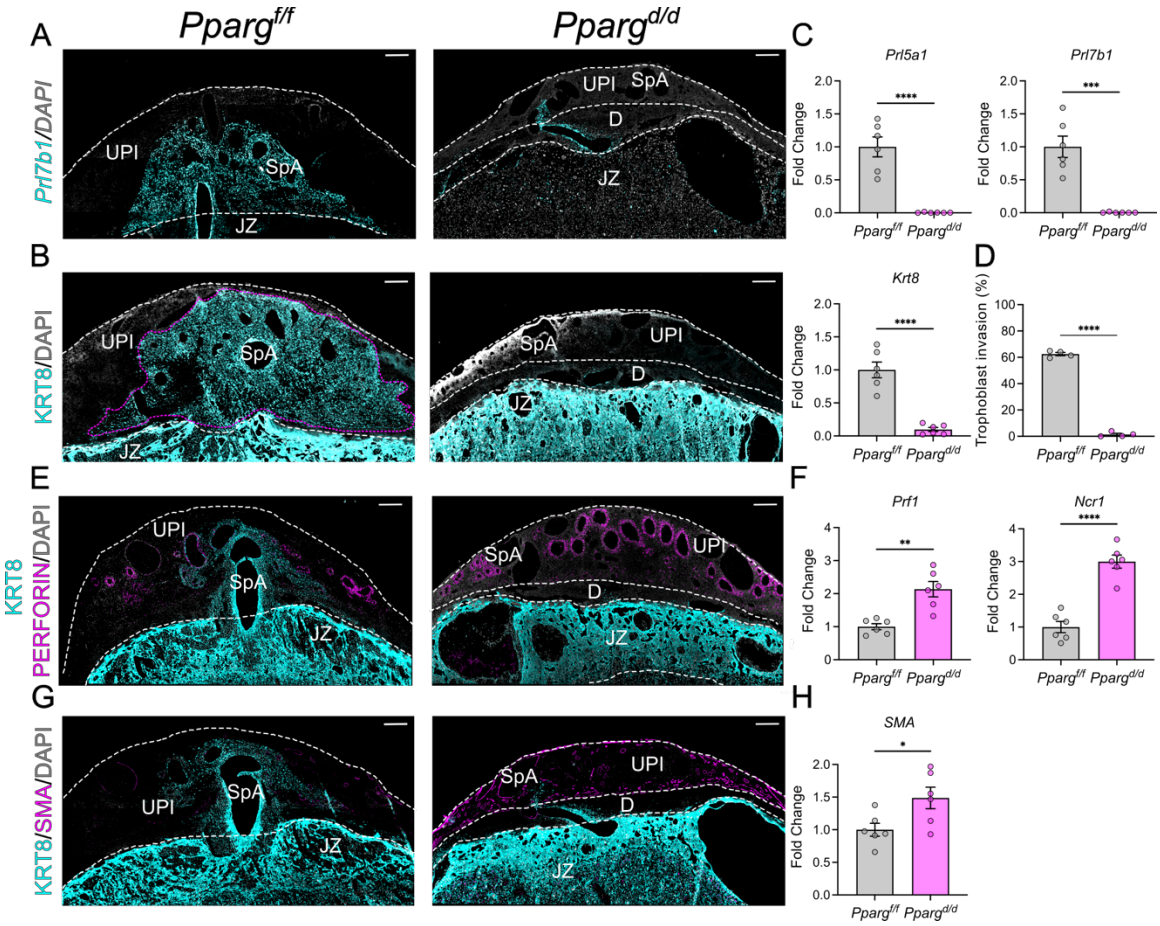

886

887 **Figure 8. Invasive trophoblast cell-specific *Pparg* disruption impacts pregnancy-**
888 **dependent transformation of the uterine-placental interface. (A)** *In situ* hybridization showing
889 *Prl7b1* transcripts (cyan) in gestation day (**gd**) 18.5 *Pparg*$^{f/f}$ and *Pparg*$^{d/d}$ placentation sites. **(B)**
890 Immunohistochemical localization of KRT8 (cyan) in gd 18.5 *Pparg*$^{f/f}$ and *Pparg*$^{d/d}$ placentation
891 sites. **(C)** RT-qPCR analysis of *Prl7b1, Prl5a1, and Krt8* expression in the uterine-placental
892 interface of gd 18.5 *Pparg*$^{f/f}$ and *Pparg*$^{d/d}$ placentation sites (n=6). **(D)** Quantification of trophoblast
893 cell invasion area (magenta dotted line) (n=4). **(E)** Immunohistochemical localization of perforin
894 (**PRF1**), a natural killer (**NK**) cell-associated protein, (magenta) and KRT8 (cyan). **(F)** RT-qPCR
895 analysis of NK cell-associated transcripts (*Prf1* and *Ncr1*) in the uterine-placental interface of gd
896 18.5 *Pparg*$^{f/f}$ and *Pparg*$^{d/d}$ placentation sites (n=6). **(G)** Immunohistochemical localization of
897 smooth muscle actin (**SMA**, magenta) and KRT8 (cyan) in the uterine-placental interface of gd
898 18.5 *Pparg*$^{f/f}$ and *Pparg*$^{d/d}$ placentation sites. **(H)** RT-qPCR analysis of *Sma* transcript in the
899 uterine-placental interface of gd 18.5 *Pparg*$^{f/f}$ and *Pparg*$^{d/d}$ placentation sites (n=6). Scale bars for
900 images in panels A, B, E and G=500 µm. Data are presented as mean ± standard error of the
901 mean. Each data point represents a distinct uterine-placental interface sample obtained from four
902 to six pregnancies. Statistical analyses were performed using unpaired *t*-tests: *$p<0.05$, **$p<0.01$,

903 ***p<0.001, ****p<0.0001. Abbreviations: UPI, uterine-placental interface; JZ, junctional zone; LZ,
904 labyrinth zone; D, decidua; SpA, spiral artery.

905